Spin coherence of a two-dimensional electron gas induced by resonant excitation of trions and excitons in CdTe/(Cd,Mg)Te quantum wells

E. A. Zhukov,[1,2] D. R. Yakovlev,[1,3] M. Bayer,[1] M. M. Glazov,[3] E. L. Ivchenko,[3] G. Karczewski,[4] T. Wojtowicz,[4] and J. Kossut[4]

[1]*Experimentelle Physik 2, Universität Dortmund, D-44221 Dortmund, Germany*

[2]*Faculty of Physics, M.V. Lomonosov Moscow State University, 119992 Moscow, Russia*

[3]*A.F. Ioffe Physico-Technical Institute, Russian Academy of Sciences, 194021 St. Petersburg, Russia*

[4]*Institute of Physics, Polish Academy of Sciences, PL-02668 Warsaw, Poland*

(Received 27 July 2007; revised manuscript received 12 October 2007; published 8 November 2007)

The mechanisms for generation of long-lived spin coherence in a two-dimensional electron gas (2DEG) have been studied experimentally by means of a picosecond pump-probe Kerr rotation technique. CdTe/(Cd,Mg)Te quantum wells with a diluted 2DEG were investigated. The strong Coulomb interaction between electrons and holes, which results in large binding energies of neutral excitons and negatively charged excitons (trions), allows one to address selectively the exciton or trion states by resonant optical excitation. Different scenarios of spin coherence generation were analyzed theoretically, among them the direct trion photocreation, the formation of trions from photogenerated excitons, and the electron-exciton exchange scattering. Good agreement between experiment and theory is found.

DOI: 10.1103/PhysRevB.76.205310 PACS number(s): 73.21.Fg, 75.75.+a, 72.25.Dc, 78.47.+p

I. INTRODUCTION

The spin coherence of electronic states is one of the key features involved in numerous concepts for spintronics devices (see, e.g., Refs. 1 and 2). It has been studied in semiconductor structures of different dimensionality, including bulklike thin films, quantum wells (QWs), and quantum dots. Accordingly, the spin coherence time of an electron has been found to vary over a wide range from a few picoseconds up to a few microseconds.

An ensemble of electron spins subject to a magnetic field is commonly characterized by three relaxation times:[3] the longitudinal spin relaxation time T_1, which is related to the relaxation of the spin component parallel to the field, and the transverse relaxation times T_2 and T_2^*. The T_2 time describes spin decoherence (i.e., relaxation of the spin components transverse to the field) of a *single* electron, while the T_2^* time describes the decoherence of the spin ensemble taking into account the inhomogeneous broadening of the electron g factor.[4,5]

The coherence time T_2 of a single spin is often few orders of magnitude longer than the dephasing time T_2^* of a spin ensemble. For example, in (In,Ga)As/GaAs quantum dots these times are 3 μs and 0.4 ns, respectively, at $B=6$ T.[6,7] A T_2^* of 300 ns has been measured in bulk GaAs by means of the Hanle effect on optically oriented electrons at liquid helium temperature.[8] For QWs the longest spin dephasing times reported so far are 10 ns for GaAs/(Al,Ga)As (Ref. 9) and 30 ns for CdTe/(Cd,Mg)Te.[11,12] They have been measured for structures with a very diluted two-dimensional electron gas (2DEG). Electron spin coherence in CdTe/(Cd,Mg)Te QWs attracts recently an increasing interest.[10–17]

Figure 1 illustrates three typical situations realized in experiments on coherent spin dynamics under resonant optical excitation of the QWs. These cases are different in the density of resident 2D electrons, n_e. In the undoped samples [panel (a), $n_e=0$] spin oriented excitons are photogenerated. Depending on experimental conditions the coherent spin dynamics of either an exciton or an electron in the exciton can be seen. However, this dynamics cannot be studied for time scales exceeding the exciton lifetime as the exciton recombination depopulates the photoexcited states. For the dense 2DEG [panel (c), $n_e a_B^2 > 1$, where a_B is the exciton Bohr radius], exciton formation is suppressed because of state-filling and screening effects. After photogeneration a hole looses its spin and energy quickly and recombines with an electron from a 2DEG. However, the spin oriented electron photogenerated at the Fermi level has an infinite lifetime which allows one to study its long-lived spin coherence and spin relaxation. In this case a circularly polarized photon can increase the spin polarization of the 2DEG by $S=\pm 1/2$. In

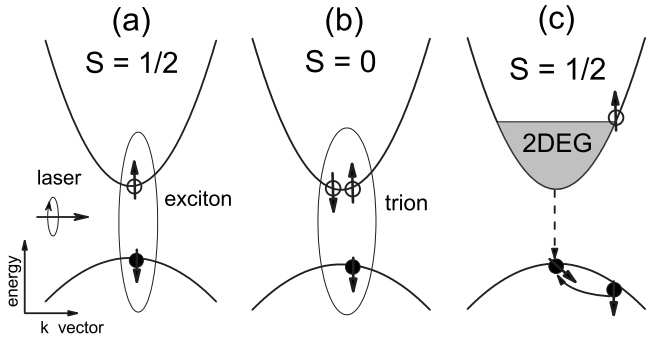

FIG. 1. Schematic presentation of generation of carrier spin coherence by circularly polarized laser pulses. The three cases differ in the density of 2DEG in the QW: (a) empty QW, only photogenerated carriers, which form excitons; (b) low density 2DEG, trions with a singlet ground state formed by a photogenerated exciton and a background electron. Interaction of the trion with the 2DEG is negligible; (c) dense 2DEG with a Fermi energy exceeding the exciton binding energy. Excitons and trions are suppressed by the 2DEG.

case of a diluted 2DEG [panel (b), $n_e a_B^2 \ll 1$] the mechanism for generation of the electron spin coherence is not so obvious.[18,19] Indeed the ground state is a singlet trion with an antiparallel orientation of electron spins. Being resonantly excited, this state would not contribute to the spin polarization because the hole undergoes fast decoherence and the total spin of the two electrons is $S=0$.

However, generation of electron spin coherence has been observed experimentally under resonant excitation of trions in QWs[11,20] and quantum dots.[6] There are two equivalent approaches to explain the generation mechanism in this case. The first one suggests that a coherent superposition of electron and trion states is excited by a circularly polarized photon when the system is subject to an external magnetic field.[6,20,21] The second one considers the 2D electrons captured for trion formation: under circularly polarized excitation electrons with a specific spin orientation will be extracted from the 2DEG and correspondingly spin polarization with the opposite sign will be induced.[11] In order to avoid the compensation of the induced spin polarization by the returning electrons after trion recombination either hole spin flip in trion or magnetic field is needed.[6]

In this paper we report on a detailed study of the coherent spin dynamics of electrons and electron-hole complexes in $CdTe/Cd_{0.78}Mg_{0.22}Te$ QWs with a low density 2DEG, performed by a pump-probe Kerr rotation (KR) technique. A theoretical analysis of the various mechanisms of spin coherence generation is carried out.

The paper is organized as follows. Section II is devoted to (i) the theoretical analysis of the physical mechanisms leading to Kerr and Faraday rotations of the probe-pulse polarization, and (ii) the theoretical description of various scenarios of electron spin coherence generation. The experimental results are presented in Sec. III, which also contains a comparison with the model considerations of Sec. II. The paper is concluded by Sec. IV in which we also comment on the specifics of *p*-doped QWs.

II. THEORY: MODEL CONSIDERATIONS

Below we underline the two main aspects of the developed theory, namely, the nature of Kerr and Faraday rotation signals and the models of spin dynamics of a 2DEG and electron-hole complexes, both trions and excitons.

In short, the basic features of an experiment designed for time-resolved measurements of the electron spin coherence can be summarized as follows: the sample containing a 2DEG is excited along the structure growth axis (z axis) by an intense pump pulse which induces resonant interband transitions. Then a much weaker, linearly polarized probe pulse with the frequency either coinciding with or different from the pump frequency arrives at the sample. The rotation of the polarization plane of the reflected or transmitted probe pulse is analyzed as a function of the delay between the pump and probe pulses. An external magnetic field B is applied in the QW plane, say, along the x axis and leads to precessions of the z and y electron spin components with the Larmor frequency $\Omega \equiv \Omega_x = g_e \mu_B B/\hbar$, where g_e is the electron in-plane g factor along the x direction and μ_B is the Bohr magneton. For 2D heavy holes bound into excitons or trions, the in-plane g factor is very small and can be ignored.[22]

A. Kerr and Faraday rotation in quantum wells

In order to describe the KR in the pump-probe experiment under normal-incidence resonant excitation we first consider the amplitude reflection coefficient of an axially symmetric single QW, which in the vicinity of the exciton or trion resonance is given by[23]

$$r_{QW}(\omega) = \frac{i\Gamma_0}{\omega_0 - \omega - i(\Gamma_0 + \Gamma)}, \tag{1}$$

where ω is the incident light frequency and ω_0, Γ_0, and Γ are the exciton (trion) resonance frequency, and the radiative and nonradiative damping rates, respectively. Taking into account also the cap layer as constituent of the heterostructure, the total amplitude reflection of the light incident on the structure from vacuum reads

$$r = \frac{r_{01} + r_{QW} e^{2i\phi}}{1 - r_{10} r_{QW} e^{2i\phi}}. \tag{2}$$

Here $r_{01} = -r_{10} = (1-n_b)/(1+n_b)$ is the reflection coefficient at the boundary between the cap layer and vacuum, n_b is the refractive index of the cap layer which for simplicity is assumed to coincide with the background refractive index of the well material, and $\phi = k_b b$, where b is the cap-layer thickness and k_b is the light wave vector in the cap layer. The above equation is valid for a spin-unpolarized system in which case the coefficient r is insensitive to the light polarization. For the spin-polarized resident electrons the reflection coefficient for right (+) and left (−) circularly polarized light has the form of Eq. (1) but r_{QW} is replaced by

$$r_{QW,\pm}(\omega) = \frac{i\Gamma_{0,\pm}}{\omega_{0,\pm} - \omega - i(\Gamma_{0,\pm} + \Gamma_{\pm})}, \tag{3}$$

with the parameters ω_0, Γ_0, and Γ dependent on the light helicity. These parameters are, in general, determined by the concentration and spin polarization of the carriers and their complexes as well as by the delay between the pump and probe pulses. When describing the Faraday rotation effect we have to analyze the amplitude transmission coefficient $t_{QW,\pm}(\omega) = 1 + r_{QW,\pm}(\omega)$. Kerr rotation signal measured in the reflection geometry is proportional to the difference

$$\Sigma_+ - \Sigma_- = \Sigma_0 \, \mathrm{Im}\{r_+^* r_-\}, \tag{4}$$

where Σ_0 and $\Sigma_\pm$ are the time-integrated intensities of the incident and reflected probe pulses in time-resolved experiments (or the stationary intensities under steady-state photoexcitation). Let us introduce the symmetrized, $\bar{r}$, and antisymmetrized, $\tilde{r}$, combinations of $r_\pm$ and assume $\tilde{r}$ to be small. Then in first approximation one obtains

$$\mathrm{Im}\{r_+^* r_-\} = \frac{-2(1 - r_{10}^2)}{|1 - r_{10}\bar{r}e^{2i\phi}|^2} \, \mathrm{Im}\left[\frac{\tilde{r}(r_{01}e^{2i\phi} + \bar{r}^*)}{1 - r_{10}\bar{r}e^{2i\phi}}\right]. \tag{5}$$

If $\bar{r}$ is also small as compared with r_{01} the right-hand side of the above equation reduces to $-2r_{10}(1-r_{10}^2)\mathrm{Im}\{e^{2i\phi}\tilde{r}\}$.

The probe at the trion resonance frequency is described by Eqs. (2)–(4), where $\Gamma_{0,\pm}$ is the oscillator strength for resonant trion excitation by $\sigma_\pm$ circularly polarized light.[24] For heavy-hole optical transitions the values of $\Gamma_{0,\pm}$ are proportional to the density of resident electrons with the spin component $\pm 1/2$, respectively.

Note that in the nonlinear regime of high excitation density the exciton-exciton interaction may play an important role in the formation of the Kerr and Faraday signals, see, e.g., Refs. 25 and 26.

In the case of a dense 2DEG the Kerr rotation angle is proportional to[29]

$$\left(\frac{e\hbar|p_{cv}|}{m_0 E_g^{QW}}\right)^2 \mathrm{Re}\left\{e^{2i\phi}\int_0^\infty d\varepsilon \frac{\mathcal{D}[f_-(\varepsilon_e)-f_+(\varepsilon_e)]}{E_g^{QW}+\varepsilon-\hbar\omega-i\hbar\Gamma_{eh}}\right\}.$$

Here $p_{cv}=\langle S|\hat{p}_x|X\rangle$ is the interband matrix element of the momentum operator, E_g^{QW} is the band gap renormalized by the quantum confinement of conduction electrons and heavy holes, Γ_{eh} is the damping rate for an electron-hole pair, m_0 is the free electron mass, ε is the sum of the 2D electron and hole kinetic energies, $\varepsilon_e=(\mu/m_e)\varepsilon$; $\mu=m_e m_{hh}/(m_e+m_{hh})$, m_e and m_{hh} are the reduced, electron and heavy-hole effective mass, respectively, $f_\pm(\varepsilon_e)$ is the energy distribution function for electrons with spin $\pm 1/2$, and $\mathcal{D}$ is the reduced density of states proportional to $\mu/\hbar^2$.

In the following we discuss, one after another, physical mechanisms of the pump-probe signal Eq. (4) for three cases of interest: (i) a diluted 2DEG subject to resonant circularly polarized photoexcitation in the singlet trion state, (ii) a diluted 2DEG with resonant generation of excitons at low temperatures favoring the binding of excitons and resident electrons into trions, (iii) exciton generation in a dense 2DEG, and (iv) a diluted 2DEG with photogeneration of carriers with kinetic energy considerably exceeding the exciton binding energy.

B. Resonant excitation of trions

We start the analysis from the case of KR by a QW with a diluted 2DEG and for resonant trion generation. In this case the radiative homogeneous broadenings $\Gamma_{0,\pm}$ (coinciding with the oscillator strength of the trion) in Eq. (3) are proportional to the concentrations of the resident electrons with spin down and spin up, see Refs. 24 and 30. Qualitatively, the physical picture looks as follows. According to the selection rules, the absorption of a circularly polarized photon leads to the formation of an electron-hole pair with fixed spin projections: $(e,-1/2;hh,+3/2)$ and $(e,+1/2;hh,-3/2)$ for right (σ^+) and left (σ^-) circularly polarized photons, respectively. At weak and moderate magnetic fields the ground state of negatively charged trions has a singlet electron configuration with antiparallel orientation of electron spins. Thus, for resonant excitation only resident electrons with orientation opposite to the photogenerated electrons can contribute to trion formation. This means that the 2DEG becomes depleted of electrons with z-spin component $S_z=+1/2$ under σ^+ pumping and of $S_z=-1/2$ electrons for σ^- pumping. An external magnetic field applied in the plane of the structure leads to precession of the spin polarization of resident electrons and, therefore, to a modulation of $\Gamma_{0,\pm}$ and oscillations of the Kerr signal. This process is shown schematically in Fig. 2.

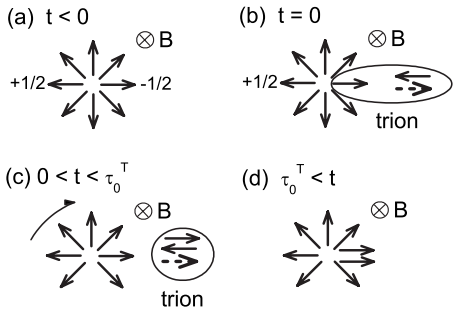

FIG. 2. Scheme of generation of 2DEG spin coherence in external magnetic fields via resonant photogeneration of trions. (a) Initial state of a 2DEG which polarization in the plane perpendicular to the magnetic field is zero. These spins are precessing around B. (b) σ^- polarized photon generates a $(e,+1/2;hh,-3/2)$ electron-hole pair, which captures a $-1/2$ resident electron to form a trion. The 2DEG became polarized due to uncompensated $+1/2$ electron spin left. (c) During trion lifetime, τ_0^T, the 2DEG polarization precesses around the magnetic field. Trion state does not precess in magnetic field as on the one hand its electronic configuration is singlet and on the other hand in-plane hole g factor is zero. (d) After trion recombination the $-1/2$ electron is returned to the 2DEG (we neglect here spin relaxation of the hole in the trion). Final state of the 2DEG with induced polarization is shown.

Now we turn to an analytical description of this scenario. The kinetic equations describing the spin dynamics of electrons and trions after resonant, pulsed excitation of trions have the form

$$\frac{dS_z}{dt}=S_y\Omega-\frac{S_z}{\tau_s}+\frac{S_T}{\tau_0^T},$$

$$\frac{dS_y}{dt}=-S_z\Omega-\frac{S_y}{\tau_s},$$

$$\frac{dS_T}{dt}=-\frac{S_T}{\tau^T}. \tag{6}$$

Here $S_T=(T_+-T_-)/2$ is the effective trion spin density with $T_\pm$ being the densities of negatively charged trions with the heavy-hole spin $\pm 3/2$, S_y and S_z are the corresponding components of the electron-gas spin density, τ^T is the lifetime of the trion spin including the trion lifetime τ_0^T and the spin relaxation time τ_s^T, i.e., $\tau^T=\tau_0^T\tau_s^T/(\tau_0^T+\tau_s^T)$, and τ_s is the electron spin relaxation time. Under normal incidence of the σ^+ polarized pump the initial conditions are $S_y(0)=0$, $S_T(0)=-S_z(0)=n_0^T/2$ with n_0^T being the initial density of photogenerated trions. Remember that the magnetic field is directed along the x axis; therefore, the x component of electron spin density is conserved.

Let us introduce the complex function $S^+(t)=S_z(t)+iS_y(t)$. It satisfies the equation

$$\frac{dS^+}{dt} = -\left(\frac{1}{\tau_s} + i\Omega\right)S^+ + \frac{S_T}{\tau_0^T}, \tag{7}$$

with the initial condition $S^+(0) = -n_0^T/2$. The solution for $S_T(t)$ is readily written as $S_T(t) = 1/2 n_0^T e^{-t/\tau^T}$. Substituting $S_T(t)$ into Eq. (7) one finds

$$S^+(t) = -\frac{n_0^T}{2}[(1-\eta)e^{-(\tau_s^{-1}+i\Omega)t} + \eta e^{-t/\tau^T}], \tag{8}$$

where $\eta = (\tau_0^T)^{-1}/[(\tau^T)^{-1} - \tau_s^{-1} - i\Omega]$. The real part of $S^+(t)$ is equal to $S_z(t)$ and given by

$$S_z(t) = \frac{n_0^T}{2}[|1-\eta|\sin(\Omega t - \Phi)e^{-t/\tau_s} - \eta' e^{-t/\tau^T}], \tag{9}$$

where

$$\Phi = \arctan[(1-\eta')/\eta''], \tag{10}$$

η' and η'' are the real and imaginary parts of η. In the particular case when electron and trion spin relaxation can be ignored, Eq. (9) is reduced to

$$S_z(t) = \frac{n_0^T}{2}[-\cos^2\Phi e^{-t/\tau^T} + \sin\Phi\sin(\Omega t - \Phi)], \tag{11}$$

where $\Phi = \arctan(\Omega\tau^T)$.

In strong magnetic field such that $\Omega T^* \gg 1$ [with $(T^*)^{-1} = (\tau^T)^{-1} - \tau_s^{-1}$] the parameter $\eta \to 0$ and $\sin\Phi \to 1$, $\cos\Phi \to 0$ yielding $\Phi \to \pi/2$. The high field asymptotics reads

$$\Phi \approx \frac{\pi}{2} - \frac{1}{\Omega\tau_0^T}. \tag{12}$$

For low magnetic fields $\Omega T^* \ll 1$ we have

$$\Phi \approx \frac{\pi}{2} - \frac{\Omega(T^*)^2}{\tau_0^T - T^*}. \tag{13}$$

The dependence of the phase Φ on magnetic field has a minimum

$$\Phi_{\min} = \arctan(2\Omega_{\min}\tau_0^T), \tag{14}$$

reached at

$$\Omega_{\min} = \frac{1}{T^*}\sqrt{1 - \frac{T^*}{\tau_0^T}}. \tag{15}$$

Note that Eqs. (14) and (15) are valid provided that τ_s is magnetic field independent. In principle, this might not be the case in the experiment, where the main contribution to the ensemble dephasing time arises from the spread of g-factor values, but for typical conditions $\tau_s \gg \tau_0^T$ so that $T^* \approx \tau_0^T$ and is almost field independent.

At zero magnetic field, the electron spin exhibits no precession, $S_y \equiv 0, S^+(t) = S_z(t)$, and one has

$$S_z(t) = -\frac{n_0^T}{2}[\eta_0 e^{-t/\tau^T} + (1-\eta_0)e^{-t/\tau_s}], \tag{16}$$

where $\eta_0 = \eta(B=0)$. This can be understood as follows. At the moment right after photoexcitation into the trion resonance by a pulsed, say, σ^- polarized light, the system contains n_0^T singlet trions with completely polarized holes $-3/2$, and n_0^T electrons with uncompensated spin $+1/2$, because the same number of electrons with spin $-1/2$ were extracted from the 2DEG to form trions. This stage is illustrated by Fig. 2(b). In the absence of spin relaxation, trions decay by emitting σ^- photons and giving back lent electrons with spin $-1/2$. As a result the initially generated electron spin polarization is compensated by the returned electrons and tends to zero as the trions vanish. It is important to note here that in the absence of spin relaxation of either trions or electrons no long-lived spin coherence of the resident electrons can be generated.

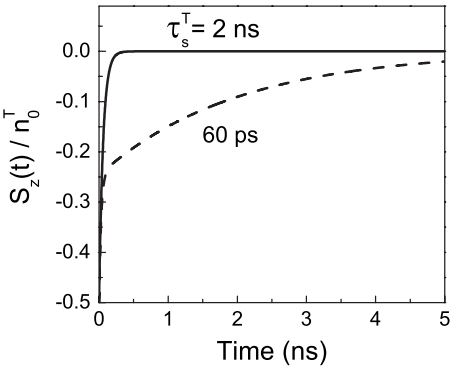

FIG. 3. Kerr signal calculated for pump and probe resonant with the trion in absence of an external magnetic field, $B=0$. The electron spin relaxation time $\tau_s=2$ ns; the trion radiative lifetime $\tau_0^T=60$ ps. The dashed curve corresponds to the trion spin relaxation time $\tau_s^T=60$ ps, while the solid curve corresponds to an unrealistically high $\tau_s^T=2$ ns. The latter situation corresponds to the compensation of the initial spin polarization by the returned electrons, $\eta_0=1$.

The compensation takes place also for the limiting case $\tau_0^T \ll \tau_s^T$, τ_s and also for the special case of $\tau_s = \tau_s^T$, see solid curve in Fig. 3. If the spin relaxation times τ_s and τ_s^T coincide, then $\eta_0=1$ and the second contribution to $S_z(t)$ proportional to e^{-t/τ_s} disappears. In this case the electron polarization $S_z(t)$ decays with the trion spin lifetime τ^T.

Spin relaxation of any subsystem brings in an imbalance, namely, the spins of the leftover and the returned electrons cannot completely compensate each other, see dashed curve in Fig. 3. The two characteristic parts of the dashed line correspond to the fast and slow negative contributions to $S_z(t)$ in Eq. (16) governed by $\tau^T=30$ ps and $\tau_s=2$ ns, respectively.

In the limit of $\tau_s \to \tau^T$, the eigenfrequencies of the system (6) are degenerate and

$$S_z(t) = -\frac{n_0^T}{2}e^{-t/\tau_s}\left(1 - \frac{t}{\tau_0^T}\right), \tag{17}$$

so that the exponential electron spin decay is modified by linear function of t.

In an in-plane external magnetic field the imbalance arises even if spin relaxation is absent or $\tau_s = \tau_s^T$. Indeed, as schematically illustrated in Fig. 2(c), both the heavy holes (due to

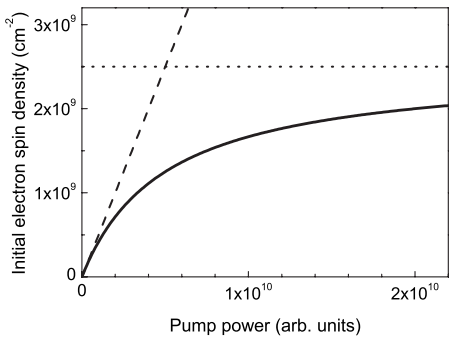

FIG. 4. Initial spin of the 2DEG as function of the pumping power (solid). The asymptotic lines correspond to linear growth (dashed) and saturation (dotted). Here it has been assumed that the laser is circularly polarized and is resonant with the trion energy. The pump power is given in units of photocreated trions in the linear regime.

their zero in-plane heavy hole g factor) and the singlet electron pairs bound in trions are not affected by the magnetic field, whereas the spins of the resident electrons precess. The trion recombines radiatively by emission of a σ^- photon and the returned electron is spin-up polarized along the z axis [Fig. 2(c)]. As a result, even after the trions have vanished ($e^{-t/\tau^T} \to 0$), the electron spin polarization is nonzero and it oscillates with frequency Ω. In Eq. (8), the η-independent term describes the spin precession of resident electrons left after the pump pulse ends while the terms proportional to η take into account the electrons left after the trions have recombined and decayed exponentially. At the moment of trion recombination, these electrons become polarized antiparallel to z, their spin is added to the total electron spin, and rotates as well with frequency Ω in the (y,z) plane.

Time-resolved KR can originate both from the electron and the trion spin polarizations. Namely, Kerr rotation angle is given by

$$\Theta_K = C_1 S_z(t) + C_2 S_T(t), \tag{18}$$

where C_1 and C_2 are constants. In particular, the constant C_1 can be obtained by the expansion of $\mathrm{Im}\{r_+^* r_-\}$ in terms of $\Gamma_{0,+} - \Gamma_{0,-}$. According to Eq. (9) the electron contribution to the Kerr signal contains both exponential monotonous and oscillatory components, whereas the trion contribution shows only a monotonous behavior, proportional to e^{-t/τ^T}. It should be stressed that the initial number of photogenerated trions under resonant excitation, n_0^T, cannot exceed $n_e/2$, where n_e is the density of the 2DEG. Thus, the factor n_0^T in Eq. (9) increases linearly with the pump intensity for small excitation density and then saturates with density increase at the value $n_e/2$. In the simplest model

$$n_0^T = \frac{n_e}{2} G\tau_0^T/(1 + G\tau_0^T), \tag{19}$$

where G is the generation rate being proportional to the pump power. Thus the initial spin polarization of the 2DEG shows a saturation behavior (see Fig. 4) which can be related to saturation of trion absorbtion.

C. Resonant excitation of excitons in a diluted two-dimensional electron gas

If the pump photon energy is tuned to the exciton transition then, at low temperatures where $k_B T < E_B^T$ (with the Boltzmann constant k_B, and the trion binding energy E_B^T), the photogenerated excitons tend to bind into trions as long as they find resident electrons with proper spin orientation. The trion thermal dissociation, on the other hand, can be neglected. Experimentally, the exciton contribution to the Kerr oscillating signal is determined by the Larmor spin precession of the electrons in the excitons. In the pump-probe experiment the correlation between the electron and hole spins via the electron-hole exchange interaction is as a rule suppressed, see Refs. 31 and 32. Therefore, the spin $\boldsymbol{s}^X$ of an electron in an exciton precesses about an in-plane magnetic field with the same frequency as that of a resident electron. Note that if the heavy holes forming excitons are unpolarized the excitons can be labeled by the electron spin $\boldsymbol{s}^X$. Moreover, the trions formed from these excitons are unpolarized as well.

At zero magnetic field the rates of an electron and an exciton binding into a trion are given by

$$\left(\frac{dn_\pm}{dt}\right)_T = \left(\frac{dn_\mp^X}{dt}\right)_T = -\gamma n_\pm n_\mp^X, \tag{20}$$

where $n_\pm$, $n_\pm^X$ are the densities of electrons and excitons with electron spin $\pm 1/2$, and γ is a constant. In addition to this constant the system is characterized by four times, namely, the exciton and trion radiative lifetimes, τ_0^X and τ_0^T, respectively, and the spin relaxation times of resident electrons (τ_s) and excitons (τ_s^X). In the presence of an in-plane magnetic field $\boldsymbol{B} \perp \mathbf{z}$, the spins of the resident electrons and the electrons in excitons precess with the same frequency Ω. In the coordinate frame which rotates around $\boldsymbol{B}$ at a rate Ω, one can apply the simple equation (20) to describe the spin-dependent decay of resident electrons and photoexcited excitons.

At low excitation intensities satisfying the condition $n_0^X \ll n_e/2$ (here n_0^X is the number of photogenerated excitons) the total spin of the electron gas after the decay of all excitons can be estimated as

$$|\boldsymbol{S}_e| = \frac{\tau^X}{2\tau_b} n_0^X, \tag{21}$$

where τ^X is the total lifetime of the exciton spin, including the radiative decay time, the time of exciton binding into a trion, $\tau_b \sim (\gamma n_e)^{-1}$, and the spin relaxation time $(\tau^X)^{-1} = (\tau_0^X)^{-1} + \tau_b^{-1} + (\tau_s^X)^{-1}$. In order to simplify the analysis we assume the time of exciton binding into a trion, $\tau_b \sim (\gamma n_e)^{-1}$, to be shorter than the exciton radiative lifetime τ_0^X and the spin relaxation time of the electron in an exciton τ_s^X. In this case, shortly after the pulsed optical excitation all excitons are bound to trions and the QW structure contains n_0^X trions and $n_e - n_0^X$ resident electrons with a total precessing spin

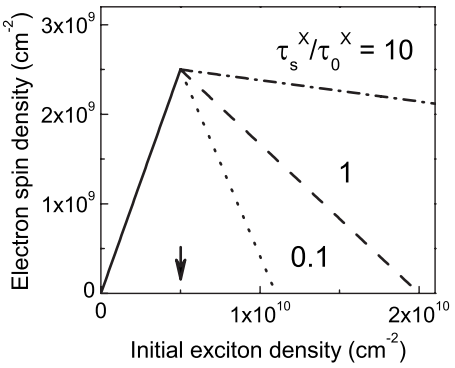

FIG. 5. Schematic plot of the spin of the 2DEG after exciton and trion recombination as a function of the initial exciton density (i.e., pumping power). The solid curve is plotted according to Eq. (22) and dotted, dashed, and dash-dotted curves are plotted according to Eq. (23). These curves correspond to different values of $\tau_s^X/\tau_0^X = 0.1$, 1, and 10, respectively. $n_e = 10^{10}$ cm^{-2}. The crossover density $n_0^X = n_e/2$ is shown by the arrow.

$$|\boldsymbol{S}_e| = n_0^X/2, \quad n_0^X \leq n_e/2. \tag{22}$$

As a result, n_0^X spins of resident electrons contribute to the Kerr rotation oscillations.

At higher excitation intensity, $n_0^X \geq n_e/2$, the spin-polarized excitons extract almost at once $n_e/2$ electrons to form trions. Therefore, in the absence of electron-in-exciton spin relaxation processes the trion density cannot exceed $n_e/2$, thus the total spin density of the electron gas is limited by $n_e/4$. The electron-in-exciton spin relaxation allows to convert the remaining $n_0^X - (n_e/2)$ excitons in trions. Obviously, the maximum number of formed trions cannot exceed the concentration of background electrons, n_e. The total spin of resident electrons after the excitons and trions have recombined can be estimated as (provided that the holes are unpolarized)

$$|\boldsymbol{S}_e| \approx \frac{1}{4}\begin{cases} n_e - \dfrac{2n_0^X - n_e}{1 + (2\tau_s^X/\tau_0^X)}, & n_e > \dfrac{2n_0^X - n_e}{1 + (2\tau_s^X/\tau_0^X)} \\ 0 & \text{otherwise.} \end{cases} \tag{23}$$

This equation is valid both for $B=0$ and $B \neq 0$ when $n_0^X \geq n_e/2$, otherwise Eq. (22) holds. At $n_0^X = n_e/2$, the values of $|\boldsymbol{S}_e|$ given by Eqs. (22) and (23) coincide and are equal to $n_e/4$.

When deriving the above equation we have neglected the spin relaxation of the resident electrons assuming $\tau_s^X \ll \tau_s$. In experiment the exciton radiative lifetime, τ_0^X, may be comparable with the trion formation time, τ_b. In this case the above estimation should be taken as a qualitative result predicting a nonmonotonous dependence of the Kerr signal amplitude on pump intensity. This nonmonotonous behavior is illustrated in Fig. 5. An initial linear growth of $|\boldsymbol{S}_e|$ followed by a linear decrease is seen. The decrease of initial electron spin as a function of pump intensity is steeper for smaller values of τ_s^X/τ_0^X, i.e., for shorter hole spin relaxation times. It is worth to stress that in this regime the electron spin polarization vanishes at very high pumping whereas, under resonant trion excitation, $|\boldsymbol{S}_e|$ monotonously increases with increasing pump power and saturates at $n_e/4$.

Detection aspects

Turning to the detection aspects, we find that selective addressing of the exciton resonance also results in temporal oscillations of the probe-pulse Kerr rotation. The modulation comes from the photoinduced difference in the resonance frequencies $\omega_{0,\pm}$ and/or the nonradiative damping rates $\Gamma_\pm$. Both $\omega_{0,+} - \omega_{0,-}$ and $\Gamma_+ - \Gamma_-$ become nonzero taking into account the exchange interaction between an electron in an exciton and the resident electrons of the 2DEG: the first difference is related to the Hartree-Fock renormalization of the electron energy in the spin-polarized electron gas, and the second one is related to the spin dependence of the electron-exciton scattering.[24] As a result, the rotation of the total spin of the electron ensemble leads to a modulation of the exciton resonance frequency and nonradiative broadening and, thus, to oscillations of the KR angle. We note that an in-plane magnetic field results also in spin precession of the electron in an exciton and the total Kerr signal will be a superposition of 2DEG and exciton signals.

The situation for the probe tuned to the trion resonance is qualitatively the same. The KR amplitude will contain components arising due to spin precession of the 2DEG and to the electron-in-exciton spin precession. However, it is expected that detection at trion resonance will be less sensitive to the exciton spin dynamics as compared to detection at the exciton resonance, see Sec. III B. We note here that the amplitude of the KR signal induced by the same number of coherent electron spins will be different for detection at the trion or the exciton energies. The difference comes from the different oscillator strengths of these resonances[24] and from the different efficiencies of signal modulation.

D. Resonant excitation of excitons in a dense two-dimensional electron gas

An increase of the 2DEG density and its Fermi level leads to dissociation of trions due to state-filling and screening effects. We consider an intermediate situation where the trions are suppressed, $n_e a_T^2 > 1$, but the excitons are not, $n_e a_B^2 \ll 1$, where a_B is the exciton Bohr radius and a_T is the characteristic trion radius. Therefore, the scenario of spin coherence generation for electrons involves two subsystems, the 2DEG and the spin-polarized excitons resonantly excited by the circularly polarized optical pulse. The electrons being initially unpolarized can gain spin polarization due to the electron-electron exchange interaction in electron-exciton flip-flop scattering processes. At zero magnetic field, the flip-flop scattering rates for the resident electrons and those bound in excitons are given by

$$\left(\frac{dn_\pm}{dt}\right)_{\text{exch}} = \left(\frac{dn_\mp^X}{dt}\right)_{\text{exch}} = -\gamma'(n_\pm n_\mp^X - n_\mp n_\pm^X), \tag{24}$$

where γ' is a constant different from γ in Eq. (20). The total number of electrons, $n_e = n_+ + n_-$, is fixed while the exciton density $n^X = n_+^X + n_-^X$ decays to zero.

Similarly to the scenario in Sec. III C, we assume that the holes in the excitons are unpolarized and the spins of both the resident and bound electrons precess with the same frequency. The Kerr rotation signal is a result of the difference in shift between the Fermi levels for spin-up and spin-down electrons and the concomitant renormalization of the resonance frequencies $\omega_{0,\pm}$ due to the exchange interaction between the spin-polarized carriers.

At weak pump intensities so that

$$\gamma n_0^X \ll \frac{1}{\tau^X} = \frac{1}{\tau_0^X} + \frac{1}{\tau_s^X} + \gamma n_e,$$

and for negligible resident-electron spin relaxation, $\tau^X \ll \tau_s$, one can use, in agreement with Eq. (21), the following estimate for the amount of resident-electron spins oriented by excitons: $|\boldsymbol{S}_e| = \frac{1}{2}\gamma\tau^X n_e n_0^X$. With increasing pump intensity the electron spin saturates at $|\boldsymbol{S}_e|_{\max} \sim \frac{1}{2} n_e (1 - \tau^X/\tau_s^X)$ when all 2DEG electrons have become spin polarized.

It should be noted that a similar description can be applied for resonant photoexcitation of excitons in the high-temperature regime where $k_B T \gg E_B^T$, but $k_B T < E_B^X$, so that the trion states are thermally unstable but the exciton bound states are still stable.

E. Nonresonant excitation of carriers

In the case of nonresonant pumping, the photogeneration of free electrons and holes is followed by their separate, uncorrelated energy relaxation toward the bottoms of the corresponding bands. The energy relaxation is accompanied by carrier spin relaxation. The holes have lost their spin after few scattering events. The total spin of the electron ensemble after energy relaxation can be estimated as

$$S_z \approx \frac{\tau_s^*}{\tau_s^* + \tau_\epsilon} n_0^e,$$

where n_0^e is the number of photogenerated electrons, τ_ϵ is the energy relaxation time, and τ_s^* is the spin relaxation time of hot electrons. We note that τ_s^* can be much shorter than the spin relaxation time τ_s of the electron gas in quasiequilibrium, entering Eq. (6).

After the particles have reached the band bottoms they can bind to form excitons and trions. In the diluted electron gas and for moderate pumping densities, the trion formation is more preferable and the subsequent spin dynamics can be described by the model in Sec. II B. At very strong pumping, when the number of photogenerated electrons exceeds that of the resident electrons, or for a dense 2DEG, for which the trions are suppressed, formation of excitons takes place. The spin dynamics in this case can be described by the scenario in Sec. II D.

F. Summary

We have developed a comprehensive model to describe the Kerr rotation signal in QWs with varying 2DEG densities and for different excitation regimes. The processes of the optical transition and spin precession are considered as separated ones.[27,28] The signal dynamics reveals spin oscillations of the resident electrons and/or of the electrons forming excitons. The pump power dependence of the Kerr rotation amplitude is as follows: at low pumping the amplitude grows linearly with the pump power, whereas in the limit of high pumping the amplitude behavior strongly depends on the excitation energy. For trion resonant excitation it saturates (as the number of generated trions is limited by half of the resident electron concentration), while for resonant excitation of excitons (at $k_B T < E_B^T$ and in the diluted 2DEG) the amplitude exhibits a nonmonotonic behavior and eventually vanishes.

A theoretical model of excitation of electron spin polarization by short laser pulses tuned to the trion resonance has been also proposed in Refs. 6, 20, and 21. Their approach is based on analysis of the temporal dynamics of the coherent quantum beats between an electron and a trion localized by a quantum dot or by well width fluctuations in a QW plane.

Our approach and the approach in Refs. 6, 20, and 21 are essentially equivalent. Indeed, let us consider a localized unpolarized electron. Its spin density matrix is diagonal with $\rho_{1/2,1/2} = \rho_{-1/2,-1/2} = 1/2$. After optical excitation with a σ_+ circularly polarized pulse a superposition state of the localized electron and a trion is formed. After the trion radiative decay the electron remains, but its density matrix is different from the initial one. For example, in the limiting case where the hole spin relaxation time is much shorter than the trion radiative lifetime which, in turn, is shorter than the electron spin relaxation time, the electron spin density matrix after trion recombination remains diagonal with

$$\rho_{1/2,1/2} = \frac{1}{2}\left(1 - \frac{|D|^2}{2}\right), \quad \rho_{-1/2,-1/2} = \frac{1}{2}\left(1 + \frac{|D|^2}{2}\right). \quad (25)$$

Here D is a complex coefficient which depends on the optical pulse parameters. The resident electron acquires spin-down polarization under pulsed σ^+ photoexcitation and a train of such pulses leads to complete spin polarization. The same single electron spin density matrix, Eq. (25), describes an ensemble where the number of spin-up electrons is smaller than that of spin-down electrons. The constant D in this case has a transparent physical sense: it characterizes the efficiency of singlet trion formation under polarized excitation of the unpolarized ensemble. One can readily check that this result is equivalent to Eq. (16) taken at $t=0$.

III. EXPERIMENTAL RESULTS

A. Experimentals

The studied $CdTe/Cd_{0.78}Mg_{0.22}Te$ QW heterostructure (031901C) was grown by molecular-beam epitaxy on an (100)-oriented GaAs substrate followed by a 2 μm CdTe buffer layer. It has five periods, each of them consisting of a 110 nm thick $Cd_{0.78}Mg_{0.22}Te$ barrier and a 20 nm thick CdTe QW. An additional 110 nm thick barrier was grown on top of this layer sequence to reduce the contribution of surface charges. The barriers contain 15 nm layers doped by iodine donors. Undoped 15 nm spacers separate the modulation-doped layers from the QWs. Electrons from the barrier donors, being collected into QWs, provide there a 2DEG with a

low density of about $n_e = 1.1 \times 10^{10}$ cm^{-2}. We have observed very similar experimental results for structures with single $CdTe/Cd_{0.7}Mg_{0.3}Te$ QWs of 12 and 8 nm widths. This confirms the general character of the reported data.

A time-resolved pump-probe Kerr rotation technique was used to study the coherent spin dynamics of the electrons.[1] We used a Ti:sapphire laser generating 1.5 ps pulses at a repetition frequency of 75.6 MHz. The laser beam was split in pump and probe beams and the time delay between the pump and probe pulses was varied by a mechanical delay line. The pump beam was circularly polarized by means of an elasto-optical modulator operated at 50 kHz. The probe beam was linearly polarized, and rotation of the polarization plane was measured by a balanced photodetector. The time-resolved Kerr rotation signal allows us to follow the evolution of the spin coherence of carriers and their complexes generated by the pump pulses. From an analysis of the decay of the Kerr rotation amplitude the spin dephasing time of the electron ensemble T_2^* can be extracted. The details of this analysis through which the mechanisms of spin dephasing of the 2DEG can be understood have been reported elsewhere.[11,17]

The Kerr rotation technique has been used in two regimes. For degenerate Kerr rotation the pump and probe beams have the same photon energy, as they originate from the same laser. This regime will be denoted as one-color experiment here. We performed, however, also a two-color experiment where the pump and probe energy can be tuned independently. For that purpose two synchronized Ti:sapphire lasers were used. Experiments were performed in magnetic fields (0–7 T) applied in the plane of the structure, i.e., in the Voigt geometry. The sample temperature was tuned in a range 1.9–100 K.

Furthermore, time-resolved photoluminescence was used to study recombination dynamics of excitons and trions. The same laser as described above was used for excitation, and time-resolved emission spectra have been recorded by a synchroscan streak camera connected to a 0.5 m spectrometer. The time resolution in this experiment was about 5 ps.

A typical photoluminescence (PL) spectrum of the QW measured at a temperature $T = 1.9$ K is shown in Fig. 6(a). It shows the exciton and trion recombination lines separated by 2 meV, corresponding to the trion binding energy. The full width at half maximum of the exciton line is about 0.5 meV and is mainly due to exciton localization on the QW width fluctuations.

The reflectivity spectrum of the same QW in the energy range of the exciton and trion resonances is given in Fig. 6(b). Following the procedure described in Ref. 24 we have evaluated the oscillator strengths of the resonances and found that the exciton oscillator strength is ten times larger than that of the trion resonance. This fact should be taken into account when the intensities of the Kerr rotation signals measured at the exciton and trion energies are compared: Firstly, the probe response is proportional to the oscillator strength and, secondly, the number of photogenerated carriers is proportional to the oscillator strength.

For interpretation of the results of the spin dynamics experiments, information on the recombination dynamics of excitons and trions under resonant excitation is necessary.

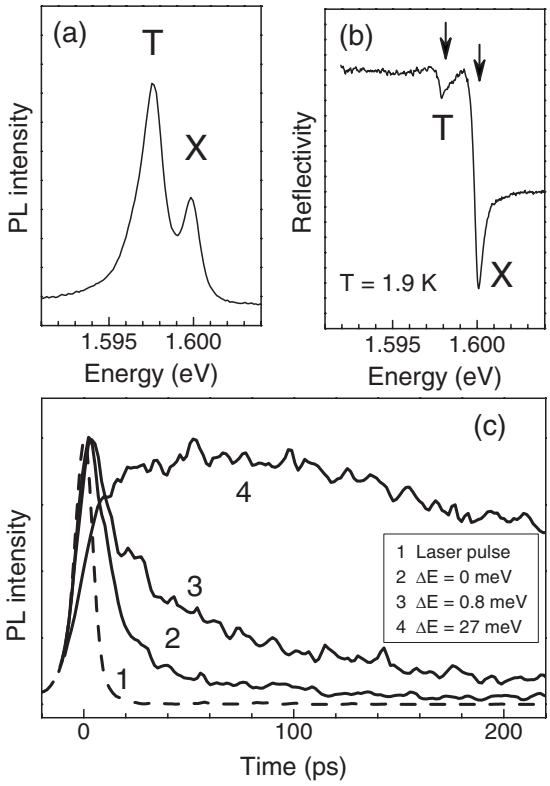

FIG. 6. (a) Photoluminescence spectrum of a 20 nm $CdTe/Cd_{0.78}Mg_{0.22}Te$ QW measured under nonresonant cw excitation with a photon energy of 2.33 eV. The exciton (X) and trion (T) resonances are separated by 2 meV, which is the trion binding energy. (b) Reflectivity spectrum of the same structure. The oscillator strength of the exciton resonance is ten times larger than the trion one. (c) Kinetics of the photoluminescence measured by a streak camera under 1.5 ps pulsed excitation resonant to the trion energy (curve 2) and detuned from it by 0.8 and 27 meV to higher energies. The dashed line shows the laser pulse.

We performed corresponding measurements under linearly polarized excitation using the streak camera for detection. The results for pumping into the exciton and trion resonances are very similar to each other. The typical recombination kinetics for the trion is given in Fig. 6(c). For resonant excitation at the trion energy (curve 2, detuning $\Delta E = 0$) about 80% of the PL intensity decays with a time of 30 ps and the rest decays with a time of 100 ps. When the excitation energy is detuned by 0.8 meV above the trion resonance a redistribution of the two exponential decays with 30 and 100 ps time occurs in favor of the longer decay component. Such a behavior is typical for QW emission.[17,35] The shorter decay time, 30 ps, can be attributed to the radiative recombination time of trions and excitons generated in the radiative cone where their wave vectors are transferred to the photons. For excitons scattered out of the radiative cone, a longer time of about 100 ps is required to be returned to the cone via emission of acoustical phonons. The exciton luminescence lifetime is slowed down to 100 ps in this case. The recombination of trions is not restricted to the radiative cone conditions as the electron left in the system can take the finite momentum to satisfy the wave vector conservation. There-

fore we may expect the fast decay of trion PL of about 30 ps even for nonresonant photoexcitation. In most cases, however, for these experimental conditions the trions are formed from photogenerated excitons, which dominate the absorption due to their larger oscillator strength. As a result the decay of the trion PL in this case is determined not by trion recombination but by trion formation, and is contributed by the exciton lifetime and trion formation time. For small detuning exemplified by curve 3, the fast 30 ps process coexists with the longer (100 ps) one. When the excitation energy is tuned to the band-to-band absorption (curve 4, $\Delta E = 27$ meV), the PL decay is extended to 250 ps as additional time is required for the free carriers to be bound to excitons. Note that the exciton binding energy in the studied QW is $E_B^X = 12$ meV.

Below we present the experimental results for the two-color and the degenerate pump-probe experiment. Furthermore, we show the experimental data for the pump power, temperature, and magnetic field dependencies of the Kerr rotation signals.

B. Two-color pump probe

The two-color Kerr rotation technique enables independent tuning of the energies of the pump and probe beams. This allows us to perform experiments with either constant excitation or detection conditions, which simplifies identification of the studied relaxation processes.

Figure 7 shows Kerr rotation signals detected at the trion and exciton resonances for three pump energies: (a) resonant with the trion, (b) resonant with the exciton, and (c) nonresonantly excited 72 meV above the exciton energy. The sample is subject to an in-plane magnetic field $B = 1$ T. All signals show damped oscillations with a frequency of 23 GHz, which is the Larmor precession frequency of the electron spins. This frequency corresponds to the Zeeman splitting of the conduction band electrons with a g-factor value of 1.64 which is in good agreement with literature data for the electron g factor in CdTe/(Cd,Mg)Te QWs.[33] Another common feature of all signals shown in Fig. 7 is the appearance of long-living spin beats which are observed beyond delays of 2.7 ns. The typical recombination times of excitons and trions do not exceed 30–100 ps for resonant and quasiresonant excitation and 250 ps for nonresonant excitation [see Fig. 6(c) and Sec. III A]; therefore, we identify the long-living signal with the coherent spin precession of the resident electrons in the 2DEG. One can see that this coherence is excited efficiently for all pump energies and can be detected by probing both the trion and exciton resonances.

Some of the signals shown in Fig. 7 contain a short-living part right after the pump pulse with a typical decay time of 50–70 ps. This part is especially pronounced for the "pump X/probe X" condition (i.e., pump and probe are degenerate with the exciton resonance), see panel (b). This fast component is related to the exciton contribution to the Kerr rotation signal, see Sec. II C and discussion below. It is in line with Ref. 9, where spin dynamics has been measured by the Hanle effect under steady-state photoexcitation. To extract the times and relative amplitudes of the short- and long-living

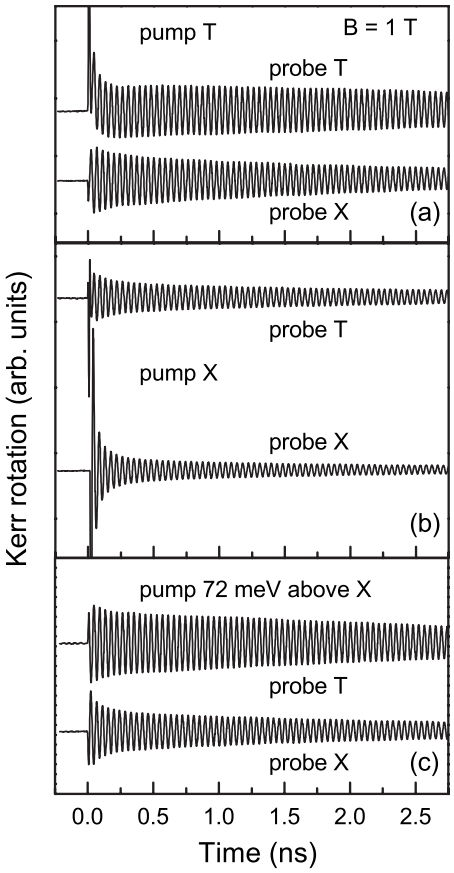

FIG. 7. KR signals measured by a two-color technique at $T = 1.9$ K, $B = 1$ T, and various pump excitation energies: (a) resonant with trion at 1.5982 eV, (b) resonant with exciton at 1.6005 eV, and (c) nonresonant at 1.6718 eV, which is 72 meV above the exciton resonance. The resonant energies for X and T are shown by arrows in Fig. 6(b). Pump density 56 W/cm^2 and probe density 8 W/cm^2.

components in the spin beat signals each trace has been fitted with a biexponential decay function

$$y(t) = (Ae^{-t/\tau_1} + Be^{-t/\tau_2})\sin(\omega t + \varphi), \tag{26}$$

where A and B are constants describing the amplitudes of the fast (τ_1) and slow (τ_2) components, respectively, ω is the Larmor frequency which is taken to be the same for both components, and φ is the initial phase.

The parameters extracted from these fits are collected in Table I. All signals, except the one for "pump T/probe T," are symmetric with respect to the abscissa. The pump T/probe T signal shows an initial relaxation of the center of gravity of the electron beats with a time constant of about 75 ps, which can be attributed to the spin relaxation time of the hole in the trions, see the second term in Eq. (9) and Ref. 11. A detailed analysis of hole spin coherence in CdTe/(Cd,Mg)Te QWs will be reported elsewhere.

The decay times and relative amplitudes in Table I are given for $B = 1$ T and $T = 1.9$ K. It is important to note that these parameters depend strongly on pump intensity, magnetic field strength, and lattice temperature. These dependencies and the underlying physical mechanisms will be dis-

TABLE I. Decay times τ_1 and τ_2 and amplitude ratios A/B extracted from biexponential fits to the experimental data using Eq. (26) in Fig. 7. $B=1$ T and $T=1.9$ K.

	Pump T	Pump X	Nonresonant
Probe T	—/5.7 ns	40 ps/3.5 ns	56 ps/3.6 ns
	0/1	0.5/0.5	0.2/0.8
Probe X	—/2.6 ns	50 ps/2.0 ns	70 ps/2.8 ns
	0/1	0.9/0.1	0.5/0.5

cussed in detail below. Here we focus our attention on the pump energy dependence of these parameters. We first concentrate on the relative amplitudes as they are a key to understanding the generation of 2DEG spin coherence and the role of the trions in this process.

For the pump T/probe T regime only the long-living electron signal of a 2DEG is observed [see panel (a) of Fig. 7]. This is in line with the model expectations as in this case only trions are photogenerated. As these trions are in the singlet ground state with antiparallel electron spins, they do not contribute to the KR signal. Moving the pump energy in resonance with the exciton and further to a band-band transition leads to appearance of the fast-decaying component for the signal probed at the trion energy. This can be attributed to the spin dynamics of the exciton which is excited either resonantly or nonresonantly, see Secs. II C and II E. The probe has a finite spectral width (about 1 meV) and tuned to the trion resonance slightly overlaps with the exciton resonance. The shortening of the electron spin dephasing time from 5.7 down to 3.5–3.6 ns is attributed to heating of the 2DEG by photocarriers with excess kinetic energy (for a detailed discussion see Secs. III D and III E).

The Kerr rotation signal probed at the exciton energy has two contributions: (i) given by the coherent precession of the electrons in excitons and (ii) given by the spin precession of the 2DEG. The former decays with the exciton recombination time. This fast exciton component is clearly seen in panels (b) and (c) and is absent for pumping at the trion resonance. For nonresonant excitation its relative amplitude does not exceed 50%. In this case electrons and holes are photogenerated 72 meV above the exciton resonance; therefore, they have a high probability to scatter and relax separately to the bottoms of their bands, where they are bound into trions and excitons. The relative amplitudes of the fast and long-lived signals reflect the probability of trion and exciton formation. It may be expected that trion formation is preferable because the 2DEG density exceeds by at least an order of magnitude the concentration of photocarriers which is in line with the experimental findings.

A very different ratio of the relative amplitudes, 90% for the fast decay and 10% for the long-living dynamics, is seen for the signal when resonantly pumped at the exciton energy and detected at the exciton [see panel (b) in Fig. 7]. There are at least two factors which favor an exciton population in comparison with a trion one under resonant pumping of the excitons. First, the photogeneration leads to formation of excitons with very low kinetic energy; therefore, they remain

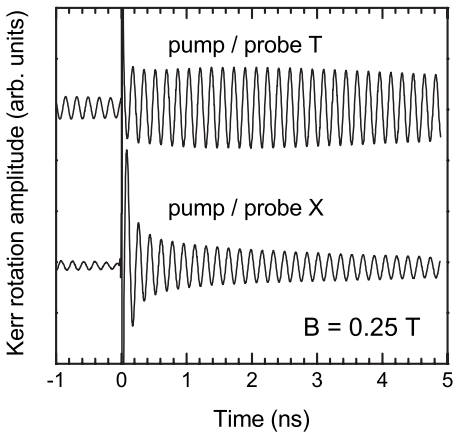

FIG. 8. Kerr rotation measured by degenerate pump-probe resonant either with the trion or the exciton energies. $T=1.9$ K, pump density is 1.5 W/cm^2 and probe density is 0.3 W/cm^2.

within the radiative cone and quickly recombine (during 30–50 ps) prior to becoming bound to trions.[35] Second, a part of excitons is localized, so that they are not mobile and cannot reach the sites in the QW where the background electrons are localized. Consequently, the formation of trions out of this exciton reservoir is suppressed. Moreover, the ratio between the contributions of the excitons and the 2DEG to the KR signal is spectrally dependent: detection at the exciton resonance is more sensitive to the spin precession of the electron in the exciton, see Sec. II C.

The results of the two-color experiments presented in Fig. 7 are in good agreement with the model expectations, namely, (i) the signal oscillating with the electron Larmor frequency is contributed by resident electrons of the 2DEG and by electrons precessing in the excitons, and (ii) trion formation resulting either from resonant photoexcitation of the trions or from capture of excitons or free carriers is a very efficient mechanism for spin coherence generation in a diluted 2DEG.

C. Degenerate pump-probe Kerr rotation

The degenerate pump-probe technique is simpler in technical realization and therefore is a more common method to address spin coherence. In this case the pump and probe pulses are generated by the same laser beam without additional spectral selection. Examples of degenerate Kerr signals can be found already in Fig. 7, for example, the pump T/probe T and pump X/probe X traces measured for coinciding energies of the two lasers.

The degenerate pump-probe signal presented in Fig. 8 was measured with the use of one laser, as will be the case for the most experiments presented in the rest of this paper. It is consistent with spin dynamics studied by two-color technique. Namely, only long-lived spin beats of resident electrons are observed when the laser is resonant with the trion and two component decay is seen for the laser hitting exciton. The experimental conditions were modified as compared with Fig. 7 in order to achieve longer electron spin coherence times. Namely, the pump density was reduced to 1.5 W/cm^2

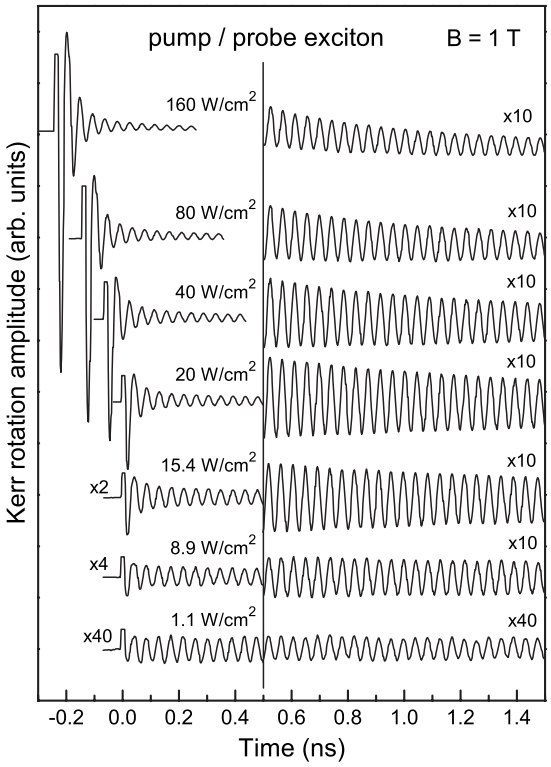

FIG. 9. Kerr rotation signals for degenerate pump-probe resonant with the exciton energy measured at different pump densities. $T=1.9$ K. For clarity of presentation upscaling factors have been used for delays exceeding 0.5 ns. Also the initial parts of the signals for pump densities exceeding 20 W/cm^2 have been shifted in time to negative delays. For all signals a coherent signal at zero delay formed due to the temporary overlap of the probe with the pump has been removed.

and a weaker magnetic field $B=0.25$ T was applied.[11] The delay time range between pump and probe in Fig. 8 covers 6 ns. Under these conditions the spin dephasing time of the resident electrons reaches 13.7 ns for pumping in the trion resonance and 4.2 ns for pumping in the exciton resonance. Moreover the spin coherence does not fully decay during the time interval of 13.2 ns between the pump pulses as is clearly seen by the beats at negative delays in Fig. 8.

D. Dependence on pump density

In this part we investigate the modifications of Kerr rotation signal occurring when the pump density is increased in a wide range of pump powers P from 1 to 320 W/cm^2. Degenerate pump-probe resonant either with the exciton or the trion transition energies is used.

Results for excitation at the exciton transition energy are collected in Fig. 9. With increase of the pump density a very different behavior is observed for the fast-decaying exciton component and the long-living 2DEG component. One can clearly see that the exciton part is rather weak at low powers, evidencing the high probability for an exciton to become bound to a resident electron and form a trion. At higher excitation power the fast-decaying component becomes more

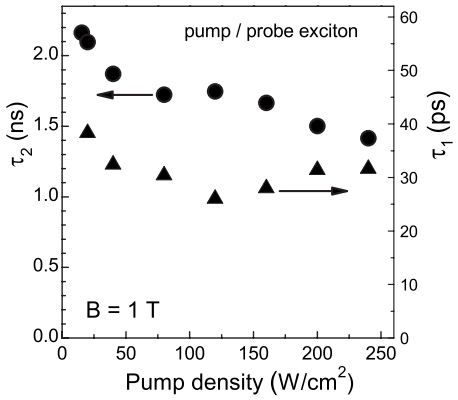

FIG. 10. Pump density dependence of the 2DEG spin dephasing time $T_2^*=\tau_2$ (circles) and the time of the fast decay τ_1 (triangles) related to the exciton recombination dynamics. $T=1.9$ K.

pronounced and even dominates in the power range $P=20-180$ W/cm^2 where the concentration of photogenerated excitons exceeds the 2DEG density. Moreover the absolute amplitude of the 2DEG signal at longer delays is decreased for pump powers exceeding 20 W/cm^2. This result will be discussed below together with the data plotted in Fig. 9.

Relaxation times obtained from the fit with Eq. (26) are given in Fig. 10. The fast-decaying component falls in the range of 25–40 ps and is independent of the pump density. It is clearly determined by the radiative recombination of excitons resonantly excited in the light cone. The decay time of the long-living component related to the spin dephasing of the 2DEG decreases from 2.1 ns at 15 W/cm^2 down to 1.4 ns at 240 W/cm^2. A possible reason for this behavior can be the heating of the resident electrons by the photoexcitation, leading to a reduction of T_2^*.

Kerr rotation signals for resonant pumping into the trion state are shown in Fig. 11. Their shape does not change markedly for varying pump densities. Only the long-living electron spin dephasing is observed, which becomes shorter for higher pump densities. The corresponding dephasing times are plotted in Fig. 12. Two characteristic regions are seen in Fig. 12: a strong decrease from 14 ns down to 4 ns at low densities, and a much slower decrease for pump densities exceeding 100 W/cm^2. The decrease of the dephasing time can be understood in terms of delocalization of the resident electrons caused by their heating due to interaction with photogenerated carriers. Thus, the electron localization in the studied samples favors longer spin dephasing times. The change of the behavior of spin dephasing times at $P\sim 100$ W/cm^2 can be attributed to saturation of the trion absorption: a further increase of the pumping intensity does not change strongly the number of photogenerated carriers.

Kerr rotation amplitudes of the 2DEG measured at the trion and exciton resonances as functions of pump density at $B=1$ T are shown by the circles in Fig. 13. The signal has been measured at a delay of 0.5 ns, where the contribution of the fast-decaying component is vanishingly small. At low excitation density both dependencies show to a good approximation a linear behavior as is illustrated by the inset. At higher excitation density the Kerr rotation amplitudes dem-

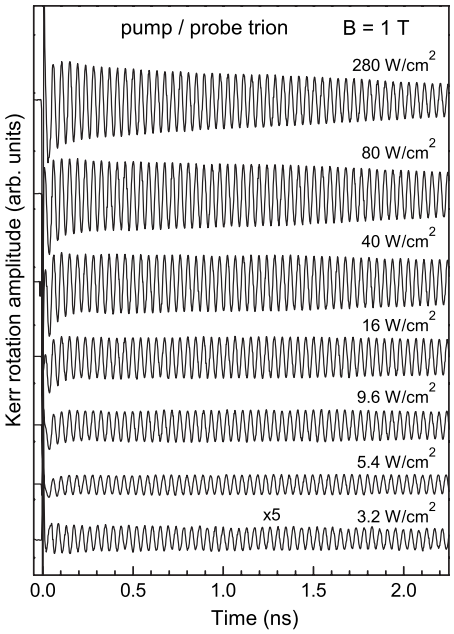

FIG. 11. Kerr rotation signals for degenerate pump-probe resonant with the trion energy measured at different pump densities. $T=1.9$ K.

onstrate pronounced nonlinear behaviors: for the "pump/probe T" configuration saturation is observed, while for the "pump/probe X" configuration the signal decreases with increase of the pump power. Both these results are in agreement with the theoretical predictions of Secs. II B and II C, respectively, as illustrated by Figs. 4 and 5. The amplitude of the fast-decaying component related to the electron-in-exciton precession in given in Fig. 13 by triangles. Note the scaling factor 0.15, which shows that this component dominates over other signals at moderate and high pump densities (see also Fig. 9).

In order to make a quantitative comparison we replot the experimental points in Fig. 13 using a different vertical scale, see Fig. 14. Namely, we normalize the Kerr signals to their

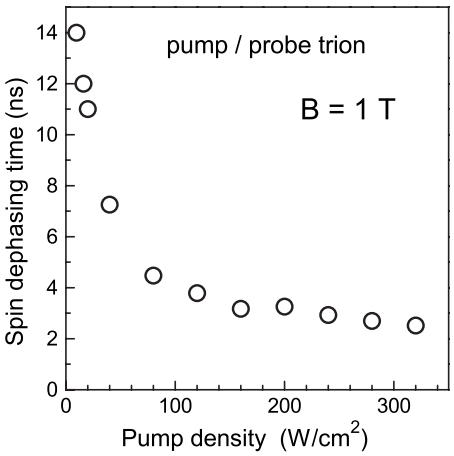

FIG. 12. Pump density dependence of the 2DEG spin dephasing time T_2^*. $T=1.9$ K.

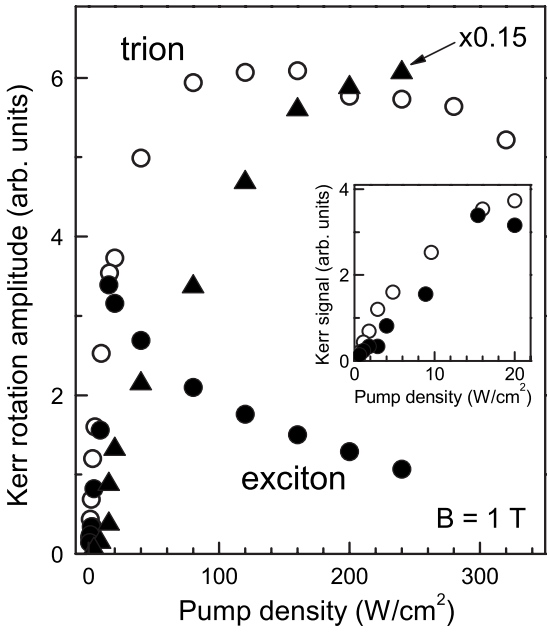

FIG. 13. Kerr rotation amplitude versus pump density for the experimental data of Figs. 9 and 11. Results for the pump resonant with the excitons and trions are shown, respectively. The amplitude of the fast-decaying component evaluated for zero delay and multiplied by a factor 0.15 is given by the triangles. The amplitudes of the long-lived 2DEG coherence measured at a delay of 0.5 ns are shown by open and closed circles for trions and excitons, respectively. The inset highlights the low density regime. $T=1.9$ K.

maximum values (which, according to our theoretical predictions, correspond to the electron spin density being equal to $n_e/4$). This allows us to compare the efficiency of spin coherence generation. One can see that in the low pumping

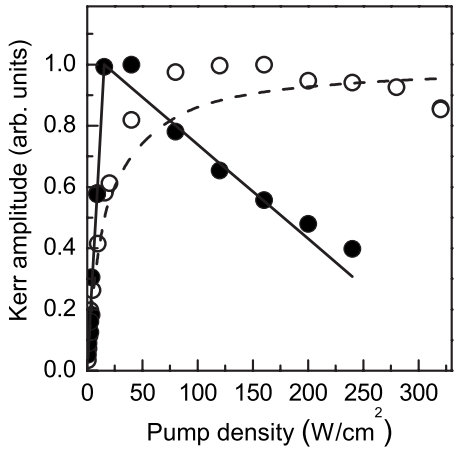

FIG. 14. Normalized long-lived amplitude of the 2DEG Kerr rotation shown in Fig. 13 measured at a delay of 0.5 ns under resonant pumping of the excitons (closed circles) and the trions (open circles). Model calculations are shown by the lines [the dashed curve has been calculated for trion resonant excitation according to Eq. (19)]. The solid lines have been calculated for excitation at the exciton frequency according to Eqs. (22) and (23). In the latter case, the fitting parameter was the ratio of τ_s^X/τ_0 which is found to be 10.

regime the spin coherence generation efficiency per absorbed photon is practically the same for the laser tuned either to the exciton or the trion resonance. This is in a good agreement with our theory: each absorbed photon creates a trion either directly or via an intermediate excitonic state, thus an electron with a given spin orientation is removed from the 2DEG. The strong pumping regime is different for exciton and trion excitations. In the case of the laser tuned to the trion resonance the spin of the 2DEG saturates (the small decrease of the Kerr rotation amplitude can be attributed to heating of the 2DEG) while for the laser tuned to the exciton resonance a strong decrease of the spin coherence generation efficiency is seen.

The curves in Fig. 14 are the results of theoretical calculations based on the models outlined in Secs. II B and II C. The dashed curve corresponds to trion resonant excitation, while the solid line is for exciton resonant excitation. For the dashed curve the only fitting parameter was the saturation level. For the solid line the only fitting parameter was the ratio between the electron-in-exciton spin relaxation time and the exciton radiative lifetime, τ_s^X/τ_0^X. The best fit corresponds to a $\tau_s^X/\tau_0^X=10$. The fact that the spin relaxation of an electron in the exciton $\tau_s^X \sim 0.5$ ns is shorter than that for the resident electrons might be due to its interaction with the hole in the exciton, which provides additional channel for spin relaxation.

E. Temperature dependence

The electron spin coherence in CdTe/(Cd,Mg)Te QWs is robust against temperature increase and can be clearly traced up to 100 K. Kerr rotation signals measured at the trion and exciton resonances in a temperature range from 1.9 up to 100 K are presented in Fig. 15. The signals are normalized to their values at zero time delay in order to highlight the trends in signal decay with increasing delay. One can see that the decay of the spin beats is thermally accelerated both for resonant pumping in the trion and in the exciton resonance, but in the former case the decrease is slower. The decay times are shown in Fig. 16. The Kerr rotation signals for the "pump/probe trion" configuration were fitted by a single exponential decay, and the resulting decay times are given in the figure by the open circles. A relatively long T_2^* time of 440 ps is measured at $T=100$ K at the trion resonance. The signals for the "pump/probe exciton" configuration were fitted by double exponential decays, see Eq. (26), for temperatures below 60 K. Above $T=60$ K only the fast component with a decay time in the 200–250 ps range is apparent. This time can be assigned to exciton recombination and we may conclude that for high temperatures the exciton spin coherence dominates over the 2DEG signal. This can be explained by a reduction of the trion formation from excitons when the 2DEG electrons have elevated kinetic energies.

We turn now to the analysis of the Kerr rotation amplitude. Its temperature dependence for trion resonant pumping is plotted in Fig. 17. The amplitude of the first maxima after the pump pulse, which closely coincides with the amplitude obtained by extrapolation to zero delay, is plotted. In the main panel the Kerr rotation amplitude is shown as a function of temperature on a linear scale. The signal rapidly looses about 80% of its intensity by a temperature increase from 1.9 up to 20 K and then gradually decreases in intensity up to 100 K, which is the maximum temperature at which signal could be recorded in experiment. The insert shows the data in a form which allows extraction of characteristic activation energies in the temperature dependence. In the temperature range from 12 to 45 K we obtain an activation energy of 2 meV, which equals to the trion binding energy.

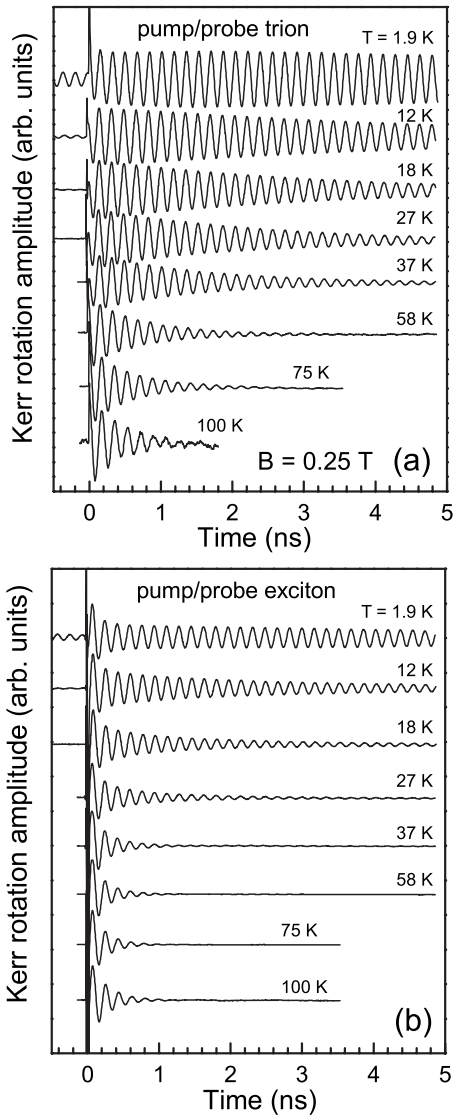

FIG. 15. Kerr rotation signal measured at different temperatures by degenerate pump-probe resonant with the trion (a) and the exciton (b). The signals are normalized on their amplitudes at zero delay. Pump density 5 W/cm^2 and probe density 1 W/cm^2.

The strong temperature dependence of the measured signals can be explained by two mechanisms: (i) delocalization of electrons and (ii) dissociation of trions. At very low temperatures $k_BT \lesssim 0.5-1$ meV, both electrons and photogenerated trions are localized in the quantum well plane by alloy fluctuations and/or interface roughnesses. The Kerr rotation signal at fixed pumping is proportional to the number of photogenerated trions. Increase of the temperature up to

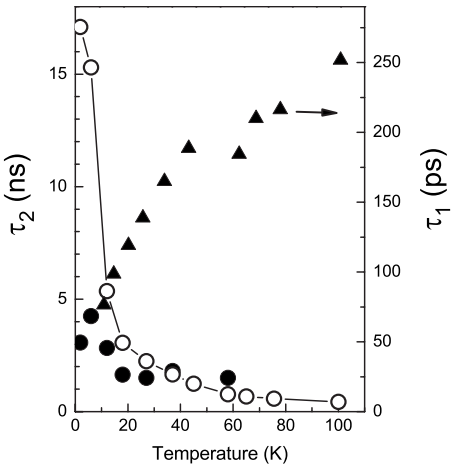

FIG. 16. Decay times determined from the Kerr rotation signals measured at different temperatures in Fig. 15. The data evaluated from a single exponential fit to the pump/probe trion data are shown by the open circles and a line as a guide to the eyes. The data for the pump/probe exciton configuration are given by the closed symbols: by the circles for τ_2 and by the triangles for τ_1. B=0.25 T, pump density 5 W/cm^2, and probe density 1 W/cm^2.

k_BT=0.5–1 meV is accompanied by electron delocalization which in turn leads to a decrease of the interaction between photogenerated electron-hole pairs and electrons. Thus, the number of photogenerated trions decreases. Furthermore, the increase of the temperature leads to thermal dissociation of trions, whose number is proportional to $\exp(-E_B^T/k_BT)$, where $E_B^T \approx 2$ meV. Thus, the trion contribution to the KR signal becomes weaker. At temperatures strongly exceeding E_B/k_B the main channel for spin coherence formation is due to exciton-electron spin-flip scattering, see Sec. II D.

F. Initial phase shift

The total spin of the electron ensemble precesses around the external magnetic field. The decay of the total spin with

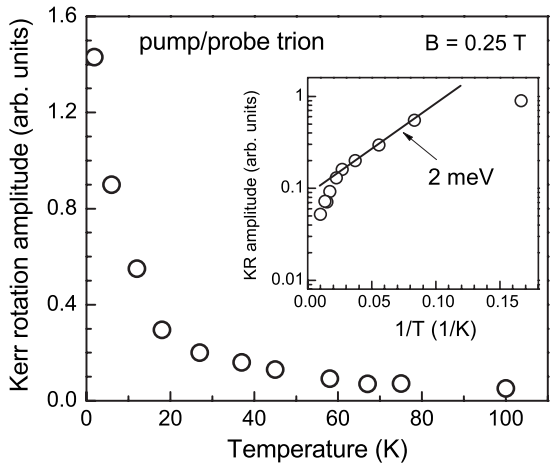

FIG. 17. Temperature dependence of the Kerr rotation amplitude of the 2DEG signals in Fig. 15(a). The inset shows a logarithmic plot of the amplitude on inverse temperature. The line corresponds to an activation energy of 2 meV.

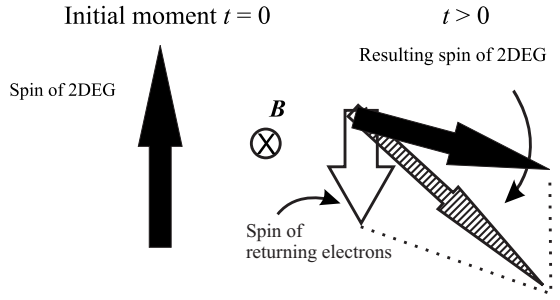

FIG. 18. Diagram explaining the phase shift of the Kerr rotation signal.

increasing delay is governed by the spin dephasing processes. The spins of the electrons forming a trion are in a singlet state and therefore do not precess around the magnetic field as the resident electrons do. Recombination of trions leads to return of the partially z-polarized electrons to the 2DEG. Their spin orientation differs from that of the precessing electrons, which results in a shift of the initial phase of the measured KR signal, see Eq. (9). This effect is illustrated in Fig. 18, where the full arrow shows the total spin of the 2DEG, while the open arrow shows the spin of the returned electrons. One can see that after trion recombination the total spin of the electron gas has been rotated by a larger angle as compared with the rotation of the resident electrons spin. This induces a phase-shift of the oscillating Kerr signal.

We have analyzed the initial phase by extrapolation of the spin beats at longer delays back toward zero delay. The experiments were performed at low excitation density with pump and probe at the trion resonance. The results are given in Fig. 19. A pronounced minimum is seen at B=0.6–0.8 T in qualitative agreement with the model calculations shown by the solid line, which was calculated with a trion lifetime τ_0^T=30 ps. We also assumed an electron spin dephasing time $\tau_s = T_2^* = 2$ ns (which corresponds to the experimental value at B=3 T). In experiment this time is longer at smaller fields. However, the calculated curve is insensitive to the choice of

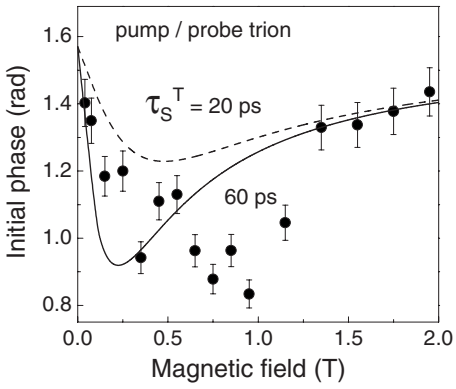

FIG. 19. Initial phase of the Kerr rotation spin beats versus magnetic field: (a) experimental data measured for degenerate pump-probe resonant with the trion. Pump density 0.64 W/cm^2 and probe density 0.5 W/cm^2. The model calculations have been performed according to Eq. (10).

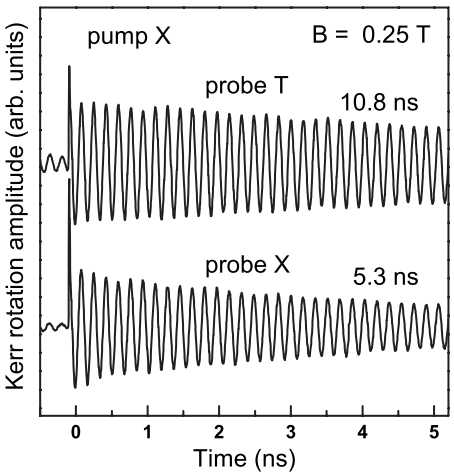

FIG. 20. Kerr rotation measured by two-color pump probe. $T=1.9$ K. Pump density 1 W/cm^2 and probe density 0.4 W/cm^2.

this value as far as τ_s remains the longest time in the system. The only free parameter in the calculations was the spin relaxation time of the hole in a trion τ_s^T. The two curves correspond to $\tau_s^T=20$ ps (dashed) and 60 ps (solid). It is seen that, in accordance with Eqs. (14) and (15), the depth of the mininum and its field position is controlled by τ_s^T. The model results demonstrate qualitative agreement with the experimental data.

G. Excitons and trions probing different resident electrons

As we have already noted above, the studied sample contains a diluted 2DEG with the Fermi energy smaller than the typical localization potential caused by well width fluctuations. As a result, at low temperatures of both the lattice and the electron gas, a major fraction of electrons is localized. We have concluded also from the pump density and temperature dependencies that the dephasing time T_2^* is strongly sensitive to electron localization, see Figs. 12 and 16. T_2^* can be extremely long for the localized electrons and shortens with electron delocalization.

To have a deeper insight into the effects of electron localization on the spin coherence we have done two-color pump-probe measurements in the regime where the longest dephasing times have been achieved, i.e., using a low pump density in a weak magnetic field of 0.25 T. Figure 20 shows the results of such an experiment, where the pump beam is resonant with the exciton transition and the Kerr rotation signal is detected at either the trion or the exciton energy. The spin dephasing times were independent of probe beam intensity when it decreased by a factor of 2 from 0.4 to 0.2 W/cm^2. Under these experimental conditions the fast-decaying component is very small for probing at the exciton energy. The excitation conditions are identical for both signals in Fig. 20, therefore, one can expect to detect the same dephasing times for the 2DEG, irrespective of the probe energy. Therefore, it is rather surprising to observe that the dephasing times of the electron coherence differ by a factor of 2: $T_2^*=10.8$ and 5.3 ns for probing at the trion and the exciton resonance, respectively.

To explain this difference we suggest that different fractions of the resident electrons contribute to the Kerr rotation signal measured at the trion or the exciton energies. This can be understood if we take into account that different mechanisms lead to Kerr rotation signal at the exciton and trion energies. For detection at the trion resonance the effect is contributed by the variation of the trion oscillator strength, which is directly proportional to the concentration of electrons with a specific spin orientation, see Sec. II A. As the in-plane localization is important to achieve stability of the trions in QWs one may expect that the trions are much more dependent on the localized electrons, which have a longer dephasing time. The Kerr rotation signal at free exciton energy monitors 2DEG spin beats mostly due to the spin-dependent exciton-electron scattering, see Sec. II C and Ref. 24. Possibility for this scattering to occur implies existence of free electrons. Therefore, at the exciton energy we address free or quasifree resident electrons which have shorter dephasing times.

IV. CONCLUSIONS

We have demonstrated experimentally the possibility to excite spin coherence of a 2DEG by resonant pumping into the trion or the exciton states, as well as by nonresonant excitation. It was shown that the time-resolved Kerr rotation signal detected experimentally at the trion and exciton frequencies contains two components: a fast contribution (which vanishes ~30 ps after the pump pulse) and a long-living one (with typical decay times of the order of nanoseconds). The fast component is related with electrons in excitons, while the long one is due to the resident electrons of the 2DEG. Experimentally we can clearly separate these contributions.

A theoretical model has been developed to describe various scenarios of spin coherence generation in QWs with a 2DEG. It is based on a classical approach to spins and accounts for resonant excitation in the trion and exciton resonances and also for nonresonant photoexcitation. A comprehensive set of experimental results is consistently described in the frame of this model.

The suggested model can be generalized to the description of spin coherence generation in a 2D hole gas. In this case the in-plane component of the heavy-hole g factor is negligible and, therefore, the regime of weak magnetic fields is realized. It can be expected that due to the stronger spin orbit interaction the free hole spin relaxation is faster than that of free electrons. On the other hand, in a low density hole gas most of the carriers are localized, so that the role of the spin orbit interaction is diminished and the hole spin relaxation times can reach up to 600 ps in GaAs/(Al,Ga)As QWs,[34] for example.

It is also worthwhile to note here, that the results of our model consideration can be also applied for describing the excitation of spin coherence in other low-dimensional semiconductor structures such as in an ensemble of singly charged quantum dots.

ACKNOWLEDGMENTS

We acknowledge fruitful discussions with Al. L. Efros, A. Shabaev, I. V. Ignatiev, and I. A. Yugova. This work was supported by the BMBF "nanoquit" program, the Deutsche Forschungsgemeinschaft (Grant No. YA 65/5-1), and by the Russian Foundation for Basic Research. E.A.Z.'s stays in Dortmund were financed by the Deutsche Forschungsgemeinschaft via Grants Nos. 436RUS17/79/04, 436RUS17/93/05, and 436RUS17/77/06. An ELI research visit to Dortmund was supported by the Gambrinus guest-professor program of the Universität Dortmund. M.M.G. was partially supported by the "Dynasty" foundation—ICFPM.

[1] *Semiconductor Spintronics and Quantum Computation*, edited by D. D. Awschalom, D. Loss, and N. Samarth (Springer-Verlag, Berlin, 2002).
[2] I. Zutic, J. Fabian and S. Das Sarma, Rev. Mod. Phys. **76**, 323 (2004).
[3] A. Abragam, *The Principles of Nuclear Magnetism* (Oxford University Press, Oxford, 1961), p. 44.
[4] X. R. Wang, Y. S. Zheng, and Sun Yin, Phys. Rev. B **72**, 121303(R) (2005).
[5] A. V. Khaetskii, D. Loss, and L. Glazman, Phys. Rev. Lett. **88**, 186802 (2002).
[6] A. Greilich, R. Oulton, E. A. Zhukov, I. A. Yugova, D. R. Yakovlev, M. Bayer, A. Shabaev, Al. L. Efros, I. A. Merkulov, V. Stavarache, D. Reuter, and A. Wieck, Phys. Rev. Lett. **96**, 227401 (2006).
[7] A. Greilich, D. R. Yakovlev, A. Shabaev, Al. L. Efros, I. A. Yugova, R. Oulton, V. Stavarache, D. Reuter, A. Wieck, and M. Bayer, Science **313**, 341 (2006).
[8] R. I. Dzhioev, B. P. Zakharchenya, V. L. Korenev, D. Gammon, and D. S. Katzer, JETP Lett. **74**, 182 (2001).
[9] R. I. Dzhioev, V. L. Korenev, B. P. Zakharchenya, D. Gammon, A. S. Bracker, J. G. Tischler, and D. S. Katzer, Phys. Rev. B **66**, 153409 (2002).
[10] P. Gilliot, D. Brinkmann, J. Kudrna, O. Cregut, R. Levy, A. Arnoult, J. Cibert, and S. Tatarenko, Phys. Rev. B **60**, 5797 (1999).
[11] E. A. Zhukov, D. R. Yakovlev, M. Bayer, G. Karczewski, T. Wojtowicz, and J. Kossut, Phys. Status Solidi B **243**, 878 (2006).
[12] H. Hoffmann, G. V. Astakhov, T. Kiessling, W. Ossau, G. Karczewski, T. Wojtowicz, J. Kossut, and L. W. Molenkamp, Phys. Rev. B **74**, 073407 (2006).
[13] G. V. Astakhov, T. Kiessling, D. R. Yakovlev, E. A. Zhukov, M. Bayer, W. Ossau, B. P. Zakharchenya, G. Karczewski, T. Wojtowicz, and J. Kossut, Phys. Status Solidi B **243**, 858 (2006).
[14] R. Bratschitsch, Z. Chen, S. T. Cundiff, E. A. Zhukov, D. R. Yakovlev, M. Bayer, G. Karczewski, T. Wojtowicz, and J. Kossut, Appl. Phys. Lett. **89**, 221113 (2006).
[15] Z. Chen, R. Bratschitsch, S. G. Carter, S. T. Cundiff, D. R. Yakovlev, G. Karczewski, T. Wojtowicz, and J. Kossut, Phys. Rev. B **75**, 115320 (2007).
[16] J. Tribollet, E. Aubry, G. Karczewski, B. Sermage, F. Bernardot, C. Testelin, and M. Chamarro, Phys. Rev. B **75**, 205304 (2007).
[17] D. R. Yakovlev, E. A. Zhukov, M. Bayer, G. Karczewski, T. Wojtowicz, and J. Kossut, Int. J. Mod. Phys. B **21**, 1336 (2007).
[18] R. I. Dzhioev, B. P. Zakharchenya, V. L. Korenev, P. E. Pak, D. A. Vinokurov, O. V. Kovalenkov, and I. S. Tarasov, Phys. Solid State **40**, 1587 (1998) [Fiz. Tverd. Tela (S.-Peterburg) **40**, 1745 (1998)].
[19] A. S. Bracker, E. A. Stinaff, D. Gammon, M. E. Ware, J. G. Tischler, A. Shabaev, Al. L. Efros, D. Park, D. Gershoni, V. L. Korenev, and I. A. Merkulov, Phys. Rev. Lett. **94**, 047402 (2005).
[20] T. A. Kennedy, A. Shabaev, M. Scheibner, Al. L. Efros, A. S. Bracker, and D. Gammon, Phys. Rev. B **73**, 045307 (2006).
[21] A. Shabaev, Al. L. Efros, D. Gammon, and I. A. Merkulov, Phys. Rev. B **68**, 201305(R) (2003).
[22] X. Marie, T. Amand, P. Le Jeune, M. Paillard, P. Renucci, L. E. Golub, V. D. Dymnikov, and E. L. Ivchenko, Phys. Rev. B **60**, 5811 (1999).
[23] E. L. Ivchenko, *Optical Spectroscopy of Semiconductor Nanostructures* (Alpha Science, Harrow, 2005).
[24] G. V. Astakhov, V. P. Kochereshko, D. R. Yakovlev, W. Ossau, J. Nürnberger, W. Faschinger, and G. Landwehr, Phys. Rev. B **62**, 10345 (2000).
[25] P. Palinginis and H. Wang, Phys. Rev. Lett. **92**, 037402 (2004).
[26] Y. Shen, A. M. Goebel, G. Khitrova, H. M. Gibbs, and H. Wang, Phys. Rev. B **72**, 233307 (2005).
[27] *Optical Orientation*, edited by F. Meier and B. P. Zakharchenja (North-Holland, Amsterdam, 1984).
[28] S. E. Economou, L. J. Sham, Y. Wu, and D. G. Steel, Phys. Rev. B **74**, 205415 (2006).
[29] A. G. Aronov and E. L. Ivchenko, Fiz. Tverd. Tela (S.-Peterburg) **15**, 231 (1973) [Sov. Phys. Solid State **15**, 160 (1973)].
[30] G. V. Astakhov, V. P. Kochereshko, D. R. Yakovlev, W. Ossau, J. Nürnberger, W. Faschinger, G. Landwehr, T. Wojtowicz, G. Karczewski, and J. Kossut, Phys. Rev. B **65**, 115310 (2002).
[31] T. Amand, X. Marie, P. Le Jeune, M. Brousseau, D. Robart, J. Barrau, and R. Planel, Phys. Rev. Lett. **78**, 1355 (1997).
[32] M. Dyakonov, X. Marie, T. Amand, P. Le Jeune, D. Robart, M. Brousseau, and J. Barrau, Phys. Rev. B **56**, 10412 (1997).
[33] A. A. Sirenko, T. Ruf, M. Cardona, D. R. Yakovlev, W. Ossau, A. Waag, and G. Landwehr, Phys. Rev. B **56**, 2114 (1997).
[34] M. Syperek, D. R. Yakovlev, A. Greilich, J. Misiewicz, M. Bayer, D. Reuter, and A. D. Wieck, Phys. Rev. Lett. **99**, 187401 (2007).
[35] V. Ciulin, P. Kossacki, S. Haacke, J.-D. Ganiere, B. Deveaud, A. Esser, M. Kutrowski, and T. Wojtowicz, Phys. Rev. B **62**, R16310 (2000).